

The glass-forming ability of model metal-metalloid alloys

Kai Zhang,^{1,2} Yanhui Liu,^{1,2} Jan Schroers,^{1,2} Mark D. Shattuck,^{3,1} and Corey S. O'Hern^{1,2,4,5}

¹*Department of Mechanical Engineering and Materials Science,
Yale University, New Haven, Connecticut, 06520, USA*

²*Center for Research on Interface Structures and Phenomena,
Yale University, New Haven, Connecticut, 06520, USA*

³*Department of Physics and Benjamin Levich Institute,
The City College of the City University of New York, New York, New York, 10031, USA*

⁴*Department of Physics, Yale University, New Haven, Connecticut, 06520, USA*

⁵*Department of Applied Physics, Yale University, New Haven, Connecticut, 06520, USA*

(Dated: March 7, 2022)

Bulk metallic glasses (BMGs) are amorphous alloys with desirable mechanical properties and processing capabilities. To date, the design of new BMGs has largely employed empirical rules and trial-and-error experimental approaches. *Ab initio* computational methods are currently prohibitively slow to be practically used in searching the vast space of possible atomic combinations for bulk glass formers. Here, we perform molecular dynamics simulations of a coarse-grained, *anisotropic* potential, which mimics interatomic covalent bonding, to measure the critical cooling rates for metal-metalloid alloys as a function of the atomic size ratio σ_S/σ_L and number fraction x_S of the metalloid species. We show that the regime in the space of σ_S/σ_L and x_S where well-mixed, optimal glass formers occur for patchy and LJ particle mixtures coincides with that for experimentally observed metal-metalloid glass formers. Our simple computational model provides the capability to perform combinatorial searches to identify novel glass-forming alloys.

Introduction

Bulk metallic glasses (BMGs) are metallic alloys that form amorphous phases with advantageous material properties [1] such as enhanced strength and elasticity compared to conventional alloys [2] and thermal plastic processing capabilities that rival those used for polymers [3]. Despite enormous progress over the past 30 years in the development and fabrication of BMGs, their commercial use has been limited due the high cost of some of the constituent elements and thickness constraints imposed by required rapid cooling. The search space for potential new BMGs is vast with roughly 46 transition metal, metalloid, and non-metal elements, which give rise to roughly 10^3 , 10^4 , and 10^5 candidate binary, ternary, and quaternary alloys, respectively.

Bulk metallic glass formers can be divided into two primary classes: metal-metal (*i.e.* transition metal-transition metal) and metal-metalloid (*i.e.* transition metal-metalloid) systems. The structural and mechanical properties [4–6] and glass-forming ability (GFA) [7] of metal-metal systems are much better understood than for metal-metalloid systems. Dense atomic packing is the key physical mechanism that determines the glass forming ability in metal-metal systems [3–6, 8], and thus these systems have been accurately modeled using coarse-grained, isotropic hard-sphere and Lennard-Jones interaction potentials [9, 10]. In contrast, since metalloid atoms form pronounced covalent interatomic bonds [11], the atomic structure that influences glass formation is not simply described by packing efficiency of spherical atoms [12]. Faithfully describing covalent bonding in simulations is challenging. *Ab-initio* simulations can de-

scribe covalent bonding accurately [13], but *ab-initio* simulations beyond tens of atoms in amorphous structures are not currently possible. Another possibility is simulations of embedded atom models that include pairwise interactions and energetic contributions from electron charge densities [11, 14]. We take a simpler geometric computational approach, where we model the covalent characteristics of metalloid atoms by arranging attractive patches on the surface of spherical particles to consider the directionality in covalently bonded structures. This *patchy particle model* has also been employed to study liquid stability [15], formation of quasicrystals [16], protein crystallization [17], and colloidal self-assembly [18, 19].

Here, we perform molecular dynamics (MD) simulations of the patchy particle model with $z = 4, 6, 8$, and 12 patches per particle that yield diamond, simple cubic, body-centered cubic (BCC), and face-centered cubic (FCC) lattices in the crystalline state. We thermally quench equilibrated liquids to low temperature at various cooling rates and measure the critical cooling rate R_c for each system. We show that the maximum GFA (minimal R_c) for patchy and LJ particle mixtures as a function of the atomic size ratio σ_S/σ_L and number fraction of the metalloid component x_S coincides with the region where metal-metalloid glass-formers are observed in experiments [20, 21]. We also used the patchy particle model to investigate the GFA in systems that form intermetallic compounds [22] since they typically do not possess FCC symmetry.

Results

In previous work [10], we showed that the slowest critical cooling rates for binary hard sphere systems occur in the range $0.8 \gtrsim \sigma_S/\sigma_L \gtrsim 0.73$ and $0.8 \gtrsim x_S \gtrsim 0.5$, which coincides with the parameters for experimentally observed metal-metal binary BMGs, such as NiNb, CuZr, CuHf, and CaAl [23–25]. Similar results hold for dense binary Lennard-Jones glasses with isotropic interatomic potentials [9]. In contrast, the metal-metalloid glass formers AuSi, PdSi, PtSi, and FeB occur at smaller σ_S/σ_L and x_S [26]. We present results from MD simulations that quantify the glass-forming ability of patchy particles as a function of the number of patches, their size, and placement on the sphere surface to model the GFA of metal-metalloid binary glass formers. (See the Methods section.)

We first consider monodisperse systems with $z = 12$ patches per particle and FCC symmetry and measure the average bond orientational order parameter $\langle Q_6 \rangle$ versus cooling rate R (using protocol 1 in the Methods section) for several patch sizes δ . For each δ , $\langle Q_6 \rangle(R)$ is sigmoidal with a midpoint that defines the critical cooling rate R_c . As R decreases toward R_c , systems with $z = 12$ form ordered Barlow packings [27] and $\langle Q_6 \rangle$ begins to increase as shown in Figure 1. In the $\delta \rightarrow 0$ limit, R_c converges to that for the Weeks-Chandler-Andersen (WCA) purely repulsive potential [28]. As the patch size increases, the 12 attractive patches promote the formation of FCC nuclei and R_c increases. For $\delta \gtrsim 0.05$ when patches begin to overlap, R_c begins to decrease because nucleation and growth of FCC clusters is frustrated by the concomitant formation of BCC and other types of nuclei. For sufficiently large δ , R_c converges to that for Lennard-Jones (LJ) systems. This nonmonotonic behavior for R_c versus δ occurs for other z as well.

We now investigate the glass-forming ability at fixed patch size $\delta = 0.1$ as a function of the number and placement of the patches for $z = 4, 6, 8$, and 12, which allows us to tune the crystalline phase that competes with glass formation. The GFA for $z = 12$ and 8 is similar. As shown in Figure 2a, $\langle Q_6 \rangle$ begins to increase for $R < R_c \approx 0.04$ with the formation of FCC and BCC clusters for $z = 12$ and 8, respectively. $\langle Q_4 \rangle$ displays a much more modest change over the same range of R . For $z = 4$, the glass competes with the formation of two interpenetrating diamond lattices [29] (Figure 2b,c), which can be detected using either $\langle Q_6 \rangle$ or $\langle Q_4 \rangle$. For $z = 6$, the simple cubic (SC) phase first forms as R decreases (indicated by a strong increase in $\langle Q_4 \rangle$), but as R continues to decrease BCC coexists with SC order (Figure 2c), which causes $\langle Q_4 \rangle$ to decrease and $\langle Q_6 \rangle$ to increase. In addition, we find that systems for which the competing crystals are more open possess lower R_c .

To model metal-metalloid glass formers, we study

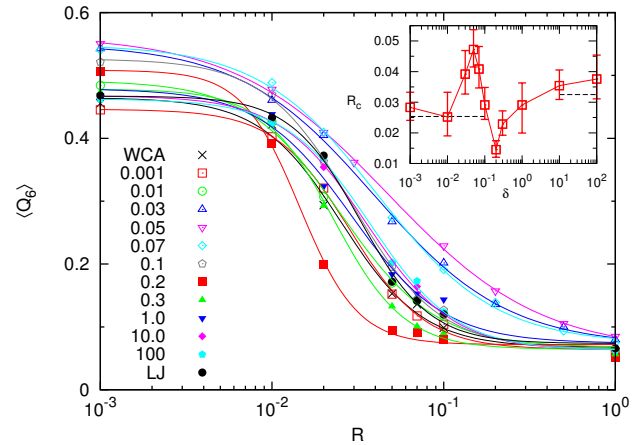


FIG. 1: **The dependence of GFA on patch size δ .** The bond orientational order parameter $\langle Q_6 \rangle$ versus cooling rate R for monodisperse patchy particles with $z = 12$ cooled at fixed reduced density $\rho^* = 1$ for several patch sizes δ . $\langle Q_6 \rangle$ was averaged over 96 separate trajectories with different initial conditions. For each δ , $\langle Q_6 \rangle(R)$ was fit to a logistic function, whose midpoint gives the critical cooling rate R_c . The inset shows R_c versus δ . The dashed horizontal lines give R_c as the patchy particle potential approaches either the LJ ($\delta \rightarrow \infty$) or WCA ($\delta \rightarrow 0$) limiting forms.

binary mixtures of isotropic LJ particles (large metal species) and $z = 4$ patchy particles (small metalloid species). We chose patchy particles with tetragonal symmetry to represent silicon atoms since they often interact with other atoms with four valence electrons in sp^3 hybridization orbitals. In Figure 3a, we show a contour plot of the critical cooling rate R_c (obtained by measuring $\langle Q_6 \rangle(R)$) as a function of σ_S/σ_L and x_S . We find two regions along the lines $x_S \sim 0.2$ and 0.8 with small values for R_c as determined by global measures of $\langle Q_6 \rangle$. However, it is also important to determine whether the patchy and LJ particles are uniformly mixed at the patchy particle number fractions $x_S \sim 0.2$ and 0.8 .

In Figure 3b, we characterize the solubility of the patchy particles within the matrix of LJ particles in glassy states created by rapid cooling to T_f using protocol 2 in the Methods section. To quantify the solubility, for each configuration, we first determine the largest connected cluster of N_c patchy particles that share faces of Voronoi polyhedra. We then calculate the radius R_c of the sphere that N_c patchy particles would assume when confined to a sphere of volume $4\pi R_c^3/3 = N_c/\rho_S$ at density $\rho_S = N_S/V_S$, where $V_S = V x_S \sigma_S^3 / (x_L \sigma_L^3 + x_S \sigma_S^3)$ and V is the volume of the cubic simulation cell. N_{sc} is the maximum number of patchy particles that can be enclosed by a sphere of radius R_c among all possible locations centered at each of the N_c patchy particles and the patchy particle solubility $f_S = N_{sc}/N_S$ can be defined for each configuration. Small values of f_S indicate that patchy particles are more likely to be neighbors with

LJ particles, not other patchy particles, while $f_S \sim 1$ indicates all patchy particles are in a spherical aggregate (Supplementary information).

Although the global bond orientational order parameter $\langle Q_6 \rangle$ indicates good glass-forming ability for LJ and patchy particle mixtures at both small ($x_S \sim 0.2$) and large ($x_S \sim 0.8$) fraction of patchy particles, we find that strong demixing of the patchy and LJ particles occurs for $x_S \sim 0.8$. Thus, when taken together, Figure 3a,b show that there is only one region in the σ_S/σ_L and x_S plane where well-mixed, good glass-formers occur: $0.2 \lesssim x_S \lesssim 0.4$ and $0.5 \lesssim \sigma_S/\sigma_L \lesssim 0.75$. This region in the σ_S/σ_L and x_S plane coincides with the region where binary metal-metalloid glass alloys (e.g. AuSi, PdSi, PtSi, and FeB) are observed. We also find similar simulation results for mixtures of tri-valent ($z = 3$) patchy and LJ particles, which mimic FeB glass-formers. In addition, the fact that ternary metal-metalloid glass formers (CoMnB, FeNiB, FeZrB, and NiPdP), for which the metal components have similar atomic sizes, also possess metalloid number fractions $x_S \sim 0.2$ supports our results [21].

It is also difficult to capture the formation of intermetallic compounds that possess particular atomic stoichiometries in each local environment using isotropic hard-sphere or Lennard-Jones potentials. We show that crystallization of intermetallic compounds can be studied efficiently using binary mixtures of patchy particles. We focus on two model intermetallic compounds: (1) an AB compound with BCC symmetry and (2) an AB_2 compound composed of hexagonal layers. We model the AB compound using a binary mixture of $z_S = z_L = 8$ patchy particles with diameter ratio $\sigma_S/\sigma_L = 0.8$ (Figure 4b). For the AB_2 compound, we consider a binary mixture of $z_L = 12$ and $z_S = 6$ patchy particles with $\sigma_S/\sigma_L = 0.5$ (Figure 4c). To encourage compound formation, we only include attractive interactions between patches on different particle species (with $\delta = 0.1$) and repulsive LJ interactions between particles of the same type. We find that the critical cooling rate R_c has a local maximum (and glass-forming ability has a minimum) at the number fraction expected for compound formation ($x_S = 0.5$ for AB and $x_S = 2/3$ for AB_2) (Figure 4a). For both AB and AB_2 , $x_S \sim 0.2$ has the smallest critical cooling rate. These results emphasize that searches for good glass-formers should avoid x_S and σ_S/σ_L combinations that yield intermetallic compound formation, which can be both stable or metastable.

Summary

We performed molecular dynamics simulations to measure the critical cooling rate R_c and assess the glass-forming ability (GFA) of patchy and LJ particle mixtures. We found several key results. First, we identified

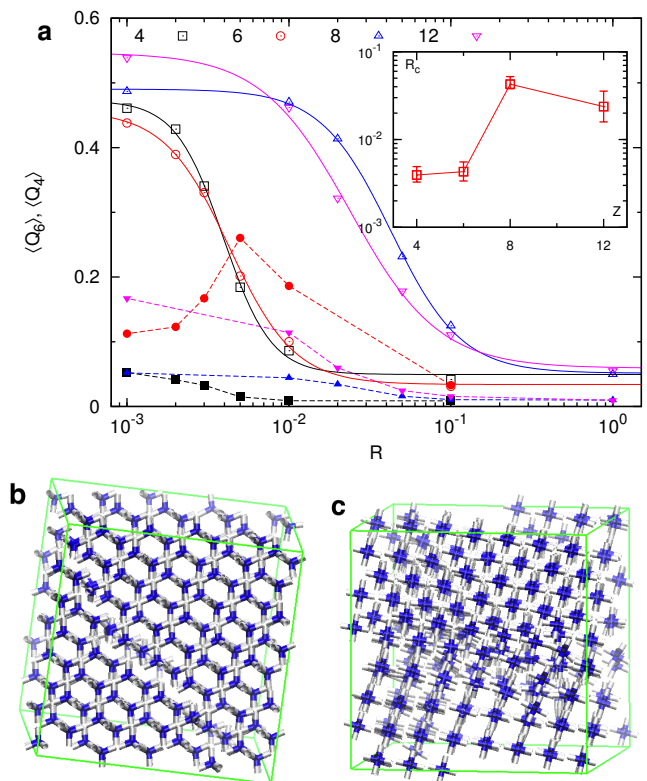


FIG. 2: **The dependence of GFA on patch number z .** **a**, Average bond orientational order parameters $\langle Q_6 \rangle$ (open symbols) and $\langle Q_4 \rangle$ (filled symbols) versus cooling rate R for monodisperse patchy particles with $z = 4$ (squares), 6 (circles), 8 (upward triangles), and 12 (downward triangles) and patch size $\delta = 0.1$. **b,c**, Ordered configurations of patchy particles in bond representation with particles colored blue and patches white: interpenetrating diamond lattices for $z = 4$ (**b**) and coexistence of simple cubic and BCC lattices for $z = 6$ (**c**).

nonmonotonic behavior in R_c as a function of the patch size δ , indicating a competition between sphere reorientation and dense sphere packing in determining GFA in the patchy particle model. Second, we tuned the number of patches per particle z and their placement on the sphere surface to vary the symmetry of the crystalline phase that competes with glass formation. We found that systems with more open lattice structures possess lower critical cooling rates. Third, we showed that the region of σ_S/σ_L and x_S parameter space where well-mixed, optimal glass-forming LJ and patchy particle mixtures occur coincides with the region where metal-metalloid glass-formers are experimentally observed. In particular, the number fraction of the metalloid species is small $x_S \sim 0.2$. The patchy particle model can also be employed to mimic the formation of intermetallic compounds, and our results emphasize that searches for good glass-formers should focus on stoichiometries that do not favor compound formation.

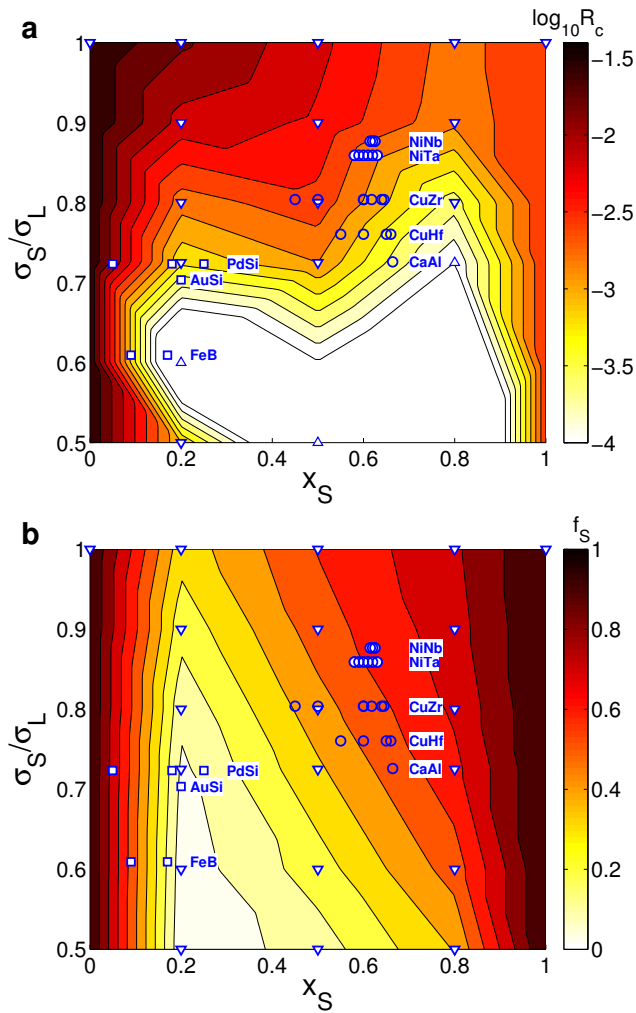


FIG. 3: **GFA in metal-metalloid systems.** **a**, Contour plot of the critical cooling rate R_c versus size ratio σ_S/σ_L and small particle number fraction x_S for a binary system composed of isotropic (large) LJ particles and (small) patchy particles with $z = 4$ and $\delta = 0.1$. Contours are interpolated using roughly 20 MD simulations (downward triangles) spread over parameter space. Known metal-metal and metal-metalloid binary glass-formers are indicated by circles and squares, respectively. **b**, Measure of the solubility (f_S) of patchy particles within the patchy and LJ particle mixtures. Number fraction f_S of patchy particles that occur in the largest connected cluster of patchy particles from glassy configurations generated at fast cooling rates ($R = 0.1$).

The search for new BMGs has largely been performed using empirical rules [30, 31] and trial-and-error experimental techniques [32]. Thus, only a small fraction of the search space of atomic species has been explored with fewer than 100 observed BMGs to date [33]. Our simple computational model for metal and metalloid atomic species provides the capability to perform more efficient and exhaustive combinatorial searches to identify novel ternary, quaternary, and multi-component glass-forming alloys. The smaller set of alloys that are predicted from

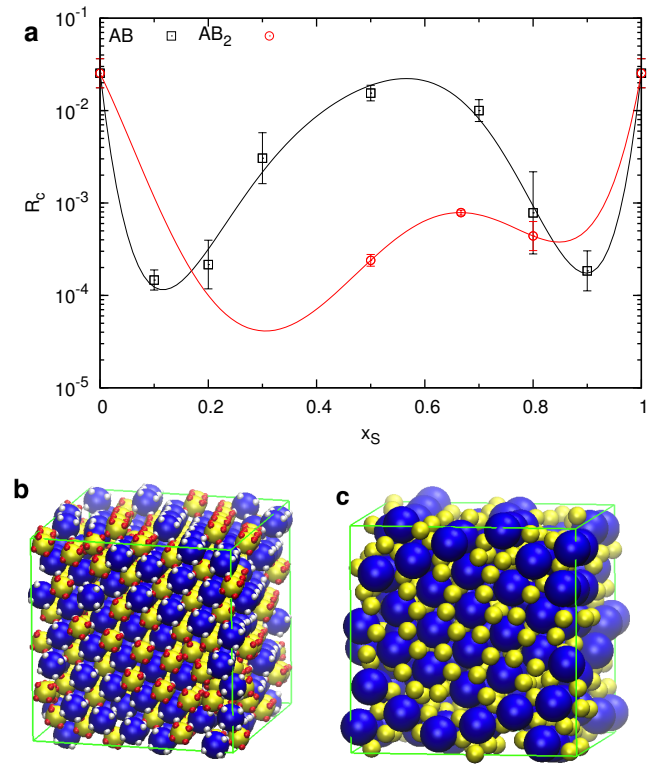


FIG. 4: **GFA in compound-forming systems.** **a**, Critical cooling rate R_c versus x_S for model AB (squares) and AB_2 (circles) intermetallic compounds. **b,c**, Intermetallic compounds formed at cooling rate (protocol 2) $R = 10^{-3} < R_c$. **b**, AB compound with $z_L = z_S = 8$ (patches are shown as small white and red bumps), BCC symmetry, and $\sigma_S/\sigma_L = 0.8$. **c**, AB_2 compound with $z_L = 12$ and $z_S = 6$ (patches not shown), stacked hexagonal planes, and $\sigma_S/\sigma_L = 0.5$.

simulations to possess slow critical cooling rates can then be tested experimentally using combinatorial sputtering [34] and other high-throughput BMG characterization techniques [35].

Methods

We performed molecular dynamics simulations [36] in a cubic box with volume V of N spherical particles of mass m decorated with z circular disks or ‘patches’ arranged on the sphere surface with a particular symmetry. Aligned patches experience Lennard-Jones (LJ) attractive interactions, whereas the particles interact via short-range repulsions when patches are not aligned. The patchy particles are bidisperse with diameter ratio $\sigma_S/\sigma_L < 1$ and number fraction of small particles x_S .

The interaction potential between patchy particles i and j includes an isotropic short-range repulsive interaction and an anisotropic attractive interaction between

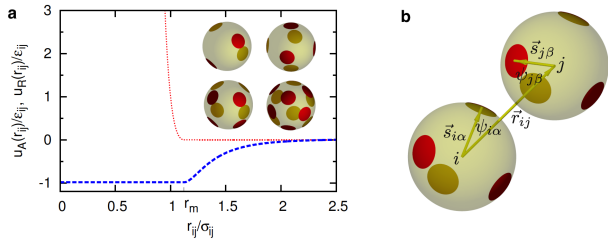


FIG. 5: **Definition of the model potential.** **a**, The purely repulsive WCA potential $u_R(r_{ij})$ is zero for $r_{ij} \geq r_m = 2^{1/6}\sigma_{ij}$ and the attractive part $u_A(r_{ij})$ of the Lennard-Jones potential is truncated and shifted so that it is zero at $r_c = 2.5\sigma_{ij}$. Here, the Lennard-Jones energy parameters are $\epsilon_{SS}/\epsilon_{LL} = \epsilon_{LS}/\epsilon_{LL} = 1$. The inset shows examples of particles with 4, 6, 8, and 12 patches with tetrahedral, simple cubic, BCC, and FCC symmetry, respectively. Red patches correspond to those on the front surface of the sphere, while dark yellow patches indicate those on the back surface. **b**, Definitions of quantities in the patchy particle interaction potential in equations (1) and (2).

patches [37]:

$$u(r_{ij}, \vec{s}_{i\alpha}, \vec{s}_{j\beta}) = u_R(r_{ij}) + u_A(r_{ij})v(\psi_{i\alpha}, \psi_{j\beta}), \quad (1)$$

where r_{ij} is the separation between particles i and j , $u_R(r_{ij})$ is the Weeks-Chandler-Andersen (WCA) purely repulsive potential [28], $u_A(r_{ij})$ is the attractive part of the Lennard-Jones potential truncated and shifted so that it is zero at $r_c = 2.5\sigma_{ij}$ (Figure 5a), the patch α on particle i has orientation $\vec{s}_{i\alpha} = (\sigma_i/2)\hat{n}_{i\alpha}$ with surface normal $\hat{n}_{i\alpha}$, and $\psi_{i\alpha}$ is the angle between \vec{r}_{ij} and $\vec{s}_{i\alpha}$ (Figure 5b). For the patch-patch interaction, we assume

$$v(\psi_{i\alpha}, \psi_{j\beta}) = e^{-\frac{(1-\cos\psi_{i\alpha})^2}{\delta_{i\alpha}^2}} e^{-\frac{(1-\cos\psi_{j\beta})^2}{\delta_{j\beta}^2}}, \quad (2)$$

which is maximized when $\psi_{i\alpha} = \psi_{j\beta} = 0$. $\delta_{i\alpha}$ gives the width of the interaction for patch α on particle i . For each patch α , we only include an interaction with the patch β that has the largest $v(\psi_{i\alpha}, \psi_{j\beta})$. In the large patch size limit, equation (2) becomes isotropic and the patchy particle model becomes identical to the full Lennard-Jones potential. In the opposite limit, as $\delta \rightarrow 0$, the patchy particle potential reduces to $u_R(r_{ij})$. We considered particles with $z = 4, 6, 8$, and 12 patches arranged on the sphere surface with tetrahedral, simple cubic, body-centered cubic (BCC), and face-centered cubic (FCC) symmetry (inset to Figure 5a). For the investigations of AB_2 compounds, we also considered systems with $z_L = 12$ and $z_S = 6$ for the large and small particles and arrangements that are compatible with the AB_2 symmetry (Supplementary information).

To assess the glass-forming ability of patchy particle systems, we measured the critical cooling rate R_c below which crystallization begins to occur. The systems are cooled using one of two protocols: (1) the temperature

is decreased exponentially in time $T(t) = T_0 e^{-Rt}$ at reduced density $\rho^* = N\sigma_L^3/V = 1.0$ from $T_0/\epsilon_{LL} = 2.0$ in the liquid regime to $T_f/\epsilon_{LL} = 0.01$ in the glassy state and (2) both the temperature and pressure p are decreased exponentially in time with $p(t) = p_0 e^{-R_p t}$, where $R_p = R$, the state point T_0/ϵ_{LL} and $p_0\sigma_{LL}^3/\epsilon_{LL} = 20$ is in the liquid regime, and the state point T_f/ϵ_{LL} and $p_f\sigma_{LL}^3/\epsilon_{LL} = 0.1$ is in the glassy regime. Protocol 2 was implemented for systems with $z < 12$ to allow the system to choose a box volume most compatible with the low-energy crystal structure. The emergence of crystalline order is signaled by a strong increase of the bond orientational order parameters Q_6 and Q_4 [38] for cooling rates $R < R_c$. We focused on systems with $N = 500$ particles, but also studied systems with $N = 1372$ to assess finite-size effects (Supplementary information). The dynamics were solved by integrating Newton's equation of motion for the translation and rotational degrees of freedom using Gear predictor-corrector methods with time step $\Delta t = 10^{-3}\sigma_{LL}\sqrt{m/\epsilon_{LL}}$ [39].

-
- [1] H. S. Chen, Rep. Prog. Phys. **43**, 353 (1980).
 - [2] A. L. Greer and E. Ma, MRS Bulletin **32**, 611 (2007).
 - [3] J. Schroers, Physics Today **66**, 32 (2013).
 - [4] D. B. Miracle, Nature Materials **3**, 697 (2004).
 - [5] H. W. Sheng, W. K. Luo, F. M. Alamgir, J. M. Bai, and E. Ma, Nature **439**, 419 (2006).
 - [6] Y. Q. Cheng, H. W. Sheng, and E. Ma, Phys. Rev. B **78**, 014207 (2008).
 - [7] A. Inoue, Acta Mater. **48**, 279 (2000).
 - [8] R. Busch, J. Schroers, and W. H. Wang, MRS Bulletin **32**, 620 (2007).
 - [9] K. Zhang, M. Wang, S. Papanikolaou, Y. Liu, J. Schroers, M. D. Shattuck, and C. S. O'Hern, J. Chem. Phys. **139**, 124503 (2013).
 - [10] K. Zhang, W. W. Smith, M. Wang, Y. Liu, J. Schroers, M. D. Shattuck, and C. S. O'Hern, Phys. Rev. E **90**, 032311 (2014).
 - [11] M. I. Baskes, Phys. Rev. Lett. **59**, 2666 (1987).
 - [12] P. F. Guan, T. Fujita, A. Hirata, Y. H. Liu, and M. W. Chen, Phys. Rev. Lett. **108**, 175501 (2012).
 - [13] S. Ryu and W. Cai, J. Phys.: Condens. Matter **22**, 055401 (2010).
 - [14] M. S. Daw and M. Baskes, Phys. Rev. B **29**, 6443 (1984).
 - [15] F. Smalenburg and F. Sciortino, Nature Phys. **9**, 554 (2013).
 - [16] J. P. K. Doye, A. A. Louis, L. R. Lin, I. Allen, E. G. Noya, A. W. Wilber, H. C. Kok, and R. Lyus, Phys. Chem. Chem. Phys. **9**, 2197 (2007).
 - [17] D. Fusco and P. Charbonneau, Phys. Rev. E **88**, 012721 (2013).
 - [18] X. Mao, Q. Chen, and S. Granick, Nature Mater. **12**, 217 (2013).
 - [19] Y. Wang, Y. Wang, D. Breed, V. N. Manoharan, L. Feng, A. D. Hollingsworth, M. Weck, and D. J. Pine, Nature **491**, 51 (2012).
 - [20] P. Ballone and S. Rubini, Phys. Rev. B **51**, 14962 (1995).
 - [21] A. Takeuchi and A. Inoue, Mater. Trans. **42**, 1435 (2001).

- [22] T. Abe, M. Shimono, M. Ode, and H. Onodera, *Journal of Alloys and Compounds* **434-435**, 152 (2007).
- [23] D. Xu, B. Lohwongwatana, G. Duan, W. L. Johnson, and C. Garland, *Acta Materialia* **52**, 2621 (2004).
- [24] L. Xia, W. H. Li, S. S. Fang, B. C. Wei, and Y. D. Dong, *J. Appl. Phys.* **99**, 026103 (2006).
- [25] Y. Wang, Q. Wang, J. Zhao, and C. Dong, *Scripta Materialia* **63**, 178 (2010).
- [26] Z. P. Lu and C. T. Liu, *Acta Materialia* **50**, 3501 (2002).
- [27] W. Barlow, *Nature* **29**, 186 (1883).
- [28] J. D. Weeks, D. Chandler, and H. C. Andersen, *J. Chem. Phys.* **54**, 5237 (1971).
- [29] D. M. Proserpio, R. Hoffmann, and P. Preuss, *J. Am. Chem. Soc.* **116**, 9634 (1994).
- [30] A. Inoue, T. Zhang, and A. Takeuchi, *Materials Science Forum* **269-272**, 855 (1998).
- [31] W. Hume-Rothery, *The Structure of Metals and Alloys* (The Institute of Metals, London, 1950).
- [32] S. Ding, Y. Liu, Y. Li, Z. Liu, S. Sohn, F. J. Walker, and J. Schroers, *Nature Mater.* **13**, 494 (2014).
- [33] A. L. Greer, *Materials Today* **12**, 14 (2009).
- [34] Y. Deng, Y. Guan, J. Fowlkes, S. Wen, F. Liu, G. Pharr, P. Liaw, C. Liu, and P. Rack, *Intermetallics* **15**, 1208 (2007).
- [35] Y. Li, Q. Guo, J. A. Kalb, and C. V. Thompson, *Science* **322**, 1816 (2008).
- [36] D. J. Evans, *Chem. Phys.* **77**, 63 (1983).
- [37] N. Kern and D. Frenkel, *J. Chem. Phys.* **118**, 9882 (2003).
- [38] P. J. Steinhardt, D. R. Nelson, and M. Ronchetti, *Phys. Rev. B* **28**, 784 (1983).
- [39] M. P. Allen and D. J. Tildesley, *Computer Simulation of Liquids* (Oxford University Press, New York, 1987).

Acknowledgments The authors acknowledge primary financial support from the NSF MRSEC DMR-1119826 (KZ). This work also benefited from the facilities and staff of the Yale University Faculty of Arts and Sciences High Performance Computing Center and the NSF (Grant No. CNS-0821132) that in part funded acquisition of the computational facilities.

Author contributions K. Z., J. S., M. D. S. and C. S. O. designed the work; K. Z. performed the simulation; K.Z. and C. S. O wrote the paper.

Additional information The authors declare no competing financial interests. Supplementary information is available online.